Journal of Materials Chemistry

Cite this: J. Mater. Chem., 2011, 21, 3646

www.rsc.org/materials

PAPER

Inhomogeneous composition of alloyed iron–platinum magnetic nanoparticles synthesized at low temperature†

Shu Chen,[ab] Donald A. MacLaren,[c] Richard T. Baker,[b] John N. Chapman,[c] Stephen Lee,[a] David J. Cole-Hamilton[b] and Pascal André*[a]

Received 21st September 2010, Accepted 6th December 2010
DOI: 10.1039/c0jm03165h

Aqueous low temperature pathways are attractive for synthesizing colloidal iron–platinum nanoparticles, which are promising candidates for applications ranging from data storage to biomedicine. Identifying the inhomogeneous composition of the products as the major hurdle of such syntheses, we present and discuss data including synthesis time, iron precursors and reducing agent aiming at quantifying and understanding the effect of the ionic precursor and the reducing agent on the composition of alloyed nanomaterials. We demonstrate that the nanoparticle composition could be modulated by using faster reducing agents as well as iron(II) salts which are less susceptible to base hydrolysis than iron(III) salts. The strategy we highlight here should be applicable to other alloy nPs fabricated by low temperature co-reduction in aqueous solution.

Introduction

Nanoparticles (nPs) have attracted considerable interest because they can display very different chemical and physical properties in comparison to bulk materials.[1–8] Their unique properties and the ability to disperse in almost any solvent offer tremendous opportunities for a wide range of chemical, physical and biomedical applications.[7–18]

Magnetic nPs often rely on making alloys containing elements such as cobalt, nickel or iron and they promise to impact biomedicine through for instance magnetic separation, targeted drug delivery, hyperthermia and Magnetic Resonance Imaging.[19] Iron–platinum (FePt) nPs are of particular importance in this regard because the face-centered-tetragonal (*fct* or $L1_0$) crystalline phase has a high Curie temperature of ~750 K and a magneto-crystalline anisotropy (K_u) of order ~6.6×10^7 J m^{-3}.[8,20,21] Thus, it seems possible to overcome superparamagnetic fluctuations at room-temperature for *fct*-nanoparticles with a diameter as small as 3 nm.[22–24] However, direct solution syntheses of well dispersed *fct*-FePt nPs are still challenging,[25,26] even if *fcc* to *fct* crystalline phase transfer can be achieved through a subsequent annealing of *fcc*-FePt nPs at high temperatures.[23,27–32]

Thermal decomposition of iron and platinum precursors, at temperatures of the order of 300 °C and above, is the most popular protocol to form *fcc*-FePt nPs,[23,32–35] with careful studies having shown that its variation can lead to the formation of iron rich shells.[36] In contrast, low-temperature syntheses have attracted less interest even though they have been successfully used to synthesize numerous types of nanoparticles with metal to semiconductor and magnetic properties.[37–48] Aqueous pathways often rely on surfactant molecules to control the nPs growth and to stabilize a water phase used to dissolve both the precursor salts and a reducing agent. nPs can then form through the exchange between water phases, with a rate that is controlled by Brownian motion and the lability of the surfactant interface.[49,50] Such an approach is attractive because of the low temperature of the synthesis, but controlling the chemical composition of alloyed nPs can prove challenging.

Only a few publications have indeed been reported on FePt nPs formation in amphiphilic systems,[51–58] and very few have focused specifically on the chemical composition of the nPs at a nanometre scale which is the target of the present work. FePt nP formation was reported in a water/cetyltrimethyl ammonium bromide (CTAB)/butanol/octane system, with $FeCl_2$ and H_2PtCl_6 salts reduced by $NaBH_4$. The average composition analyzed by transmission electron microscopy (TEM) and Energy Dispersive X-ray (EDX) spectroscopy appeared to follow the molar ratio of the precursors.[53] A water/triton/cyclohexane system was also shown to lead to FePt and $FePt_3$ nPs obtained by $FeCl_2$ and H_2PtCl_6 co-reduction by hydrazine monohydrate.[54] In both studies, TEM indicated that the nPs are polydispersed and aggregated, while no detailed composition data at a nanoscale

[a]*SUPA, School of Physics and Astronomy, University of St Andrews, St Andrews, Fife, KY16 9SS, UK. E-mail: Pascal.Andre@st-andrews.ac.uk*
[b]*EaStCHEM, School of Chemistry, University of St Andrews, St Andrews, Fife, KY16 9ST, UK*
[c]*SUPA, School of Physics and Astronomy, The University of Glasgow, Glasgow, G12 8QQ, UK*

† Electronic supplementary information (ESI) available: Details of the FePt nanoparticles syntheses, experimental characterization and original spectra including SQUID, XRD, TEM and nanoSTEM-EDX. See DOI: 10.1039/c0jm03165h

were presented.[53,54] In a water/isooctane/Brij/butanol system the size of the nPs synthesized with anhydrous hydrazine could be controlled by adjusting the hydration of the surfactant and the composition appeared to be controlled by tuning the initial ratio of precursors, K_2PtCl_4 and $FeCl_3$.[55] However, the purpose of that publication was not to provide insight into compositional variations between individual nPs.

In the present study, we highlight such variations as a crucial consideration when reporting on FePt nPs synthesized at low temperature, and in contrast with traditional literature, we present and discuss many of the problems of this synthetic pathway with the aim of identifying suitable strategies to overcome them. A detailed investigation focusing on the stoichiometry and the composition of FePt nPs is presented associated with a precise composition analysis of individual nPs revealing a strong inhomogeneous distribution of Fe and Pt between particles. Reaction time, precursor ions and reducing agents were used to gain insight into the mechanisms associated with the insertion of iron atoms into the Fe_xPt_{1-x} nPs. Limiting parameters including iron salts hydrolysis and a mismatch in the co-reduction kinetics of the two salts could then be identified. These results indicate that, to overcome these problems and obtain higher stoichiometry in FePt nPs by co-reduction at low temperature, future investigations should focus on preventing the formation of hydrolytically unstable iron complexes, preferably by working in the absence of water. While we illustrate that the experimental results regarding the composition Fe_xPt_{1-x} nPs can be deceptive, the knowledge gained and herein presented should be applicable to the synthesis of other alloys.

Experimental results

A non-ionic surfactant, Brij52, was chosen to reduce the impact of reducing the precursor ions, hence altering the ionic content over the course of the synthesis. It consists of a hydrophobic block of a 16 carbon long alkyl chain and a hydrophilic head including 2 ethylene oxide units terminated by a hydroxyl group (Fig. 1A). The phase behavior of the precursor free water/isooctane/Brij52/butanol amphiphilic system was characterized by impedance spectroscopy. As shown in Fig. 1B, the impedance spectra, $Z = f(Z',Z'')$, are each dominated by semicircular features for all the hydration values, $w = [H_2O]/[surfactant] = 1$ to 6, defined as the ratio of water molecule per surfactant.[59] The diameter of the semi-circles is related to the resistance of the system and the spectra were fitted to extract these resistance values. Conductivity values were calculated from these and follow a non-monotonic behavior with the hydration, w, of the system (Fig. 1C). The conductivity indeed first increases with w, reaches a maximum at $w = 4$, and then decreases at higher hydration. Up to $w = 4$, conductivity values reflects an increased salt content associated with the hydration,[59] the variation of the rigidity of the surfactant interface, and consequently the variation of the exchange rate of the water phases in the amphiphilic system. Above $w = 4$, the system becomes unstable and progressively phase separates into an upper phase rich in oil and a lower phase rich in water. The solution was kept under stirring over the 3 h duration of the syntheses which were then completed at $w = 4$, corresponding to the maximum of the conductivity values to optimize the exchange rate (Fig. 1C).

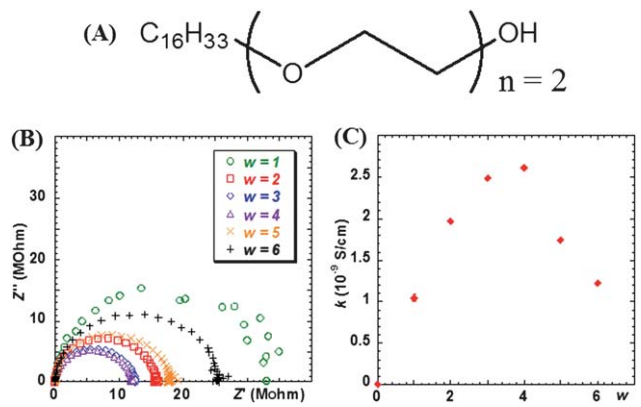

Fig. 1 Chemical structure of Brij52 non-ionic surfactant (A). Plot of real (Z') *vs.* imaginary (Z'') components of complex impedance of water/isooctane/Brij52/butanol amphiphilic system measured at 30 °C, [Brij52] = 0.3 mol L^{-1}, [Brij52]/[butanol] = 5, hydration, w = 1(○), 2 (□), 3 (◇), 4 (△), 5 (×) and 6 (+) (B). Conductivity variation as a function of water content, w (C).

In a typical synthesis, a surfactant solution was prepared by mixing isooctane, Brij52 and butanol in a surfactant to alcohol molar ratio of 5 : 1. Dissolution was obtained after 15 min sonication. Aqueous stock solutions of platinum and iron were added to the amphiphilic system to obtain the desired $[Pt^{2+}]$ and $[Fe^{3+}]$ concentrations, respectively. 30 min sonication was then applied, followed by injection of the reducing agent to reach the targeted molar ratio of [reducing agent] to [Fe + Pt]; the final w value was reached after addition of the hydrated reducing agent solution. The system was stirred at 30 °C for 3 h. Dodecane thiol was then injected and the solution aged for a further 15 min. The nPs were then precipitated by adding alcohol and next collected by centrifugation. This extraction step was repeated several times. A similar protocol was followed when the syntheses were completed with different iron and platinum precursors, and different reducing agents. A detailed example of nPs preparation protocol is given in the ESI†. For the sake of clarity and to keep this manuscript concise, the list of chemical grades and providers together with the description of characterization techniques are provided in the ESI†.

To tune the composition of the nPs, syntheses were completed with variation of the initial precursor molar ratio incrementing the concentration of $FeCl_3$ whilst keeping the concentration of K_2PtCl_4 constant.[59] The particles were then synthesized with precursor salt ratios, Fe : Pt, ranging from 0.2 to 1.8. To quantify the average composition of the nPs, the product of each synthesis was dissolved in *aqua regia* solution and the ratio of Fe to Pt elements in the final solution was determined by Inductively Coupled Plasma Optical Emission Spectrometry (ICP-OES,[59] Fig. 2A). All the results are reproducible and very consistent from one sample to another.

The final nP stoichiometry appears to correlate perfectly with the initial ratio of precursor salts. This is illustrated by the linear variation of the ICP-OES composition as a function of the initial precursor molar ratio in the synthetic media which reveals an apparent ability to control the global composition of FePt nPs (Fig. 2A). Wide-angle powder X-ray diffraction (XRD)[59] patterns are characteristic of FePt nPs with a face centre cubic (*fcc*) crystalline structure (Fig. 2B) with the peaks lying around

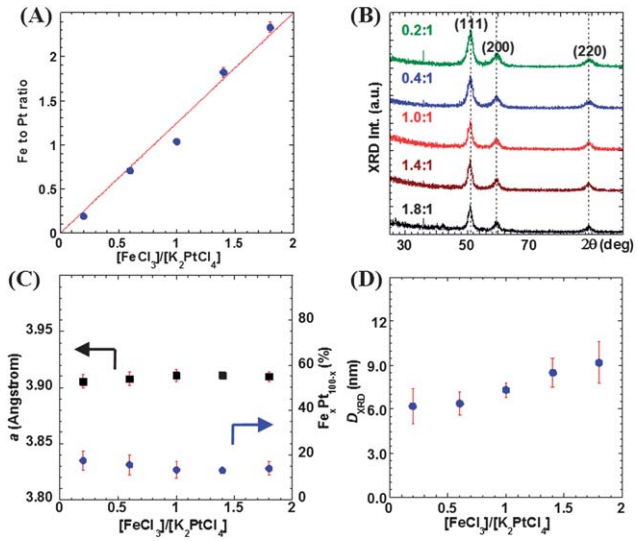

Fig. 2 FePt nPs synthesized with varied $FeCl_3$ concentration at 30 °C in isooctane, [Brij52] = 0.3 mol L^{-1}, [Brij52]/[butanol] = 5, w = 4 and $[N_2H_4 \cdot H_2O]/[Fe^{3+} + Pt^{2+}]$ = 40. (A) Composition analysis by ICP-OES, (B) XRD patterns, (C) lattice constant (■) and chemical composition (●) and (D) crystalline grain size, *i.e.* diameter, (D_{XRD}) as a function of Fe to Pt ratio in the syntheses.

51°, 60° and 89° arising from the (111), (200) and (220) diffraction. It is, however, noticeable from Fig. 2B that the position of the XRD peaks and the implied lattice constant remain independent of the relative iron and platinum precursor concentrations.[59] This is in contradiction to the ICP-OES results of Fig. 2A since the composition change suggested by ICP-OES should manifest as a shift of peaks towards higher 2θ values and a simultaneous reduction of the lattice constant with increased Fe content (Fig. 2C).[60] In contrast to the known lattice constant of $Fe_{50}Pt_{50}$ (~3.834 Å), the values for all the samples appear to be close to 3.910 Å. When compared with the lattice constant of Pt metal (~3.930 Å), this suggests a fixed Fe composition of about 15% across the entire set of samples (Fig. 2C). Electron diffraction data (ESI, Fig. S4†) yield similar information. Fig. 2D illustrates the increase of the crystalline size with the Fe to Pt precursor ratio and Table 1 summarizes all these results.

The apparent contradiction between ICP-OES and XRD datasets can be resolved by TEM,[59] (Fig. 3) which reveals that the product of the reaction is inhomogeneous and presents well-defined Pt-rich nanoparticles together with larger fragments of multidomains made of Fe-rich materials. In Fig. 3, the first two columns on the left-hand side show low magnification TEM pictures and large length scale nP areas, while the two columns on the right-hand side display higher resolution and magnification TEM images. The $FeCl_3$ to K_2PtCl_4 molar ratio is tuned from 0.2 to 1.8 (Fig. 3A–E). Fig. 3A presents TEM characterization of FePt synthesized with an initial $[FeCl_3]$ to $[K_2PtCl_4]$ ratio of 0.2. Individual nPs are associated with a film-like material (Fig. 3A1), while two distinct populations of nPs appear in Fig. 3B: small size nPs are smaller than 10 nm in diameter which is close to the XRD diameter of 6.2 nm (Table 1). nPs larger than 10 nm appear to be aggregated and fused together (Fig. 3A2). Fig. 3A3 and A4 present higher magnification TEM of the nPs and the film material, respectively. All the samples presented in Fig. 3 agree well with such description and the common features in all samples can be summarized as follows.

(i) The nPs of high contrast are fairly well dispersed and are mixed with a film-like material of weaker contrast, which could also be amorphous. The nPs are polydisperse in size and shape, with a similar structure and morphology regardless of the Fe to Pt precursor ratio (1st and 2nd columns).

(ii) The dark contrast nPs have knobby like morphology and appear to be polydomain, probably resulting from the coalescence of smaller nPs during synthesis (3rd column).

(iii) The particles increase in size with increasing the initial $[FeCl_3]$ concentration while the size distributions broaden (ESI, Fig. S3†). This trend would be consistent with the XRD data presented in Table 1 (3rd column), even though the crystalline diameters only show a very small variation when considered in the light of the experimental uncertainties also presented in the 3rd column of Table 1.

(iv) High magnification TEM images illustrate the formation of the film-like material of lower electronic contrast (4th column).

Elemental analysis by Energy Filtered TEM (EFTEM) image and nanometre scale Scanning Transmission Electron Microscopy and Energy Dispersive X-ray (nanoSTEM-EDX) analysis[59] were completed to complement both ICP-OES and XRD data, by providing the composition of the Fe_xPt_{1-x} nPs at a nanometre scale. Fig. 4A1 corresponds to a regular bright field TEM image and displays the same duality as reported in Fig. 3 with a coexistence of higher contrast nPs and a lower contrast film-like material, while Fig. 4A2 is the EFTEM image of the same area, showing Pt in blue and Fe in red. The dark discrete particles of Fig. 4A1 are Pt-rich whilst the lighter material is Fe-rich. Fig. 4B1 and B2 are nanoSTEM-EDX analysis from a large set of nPs and single nP, respectively. The red squares in Fig. 4B indicate the areas where nanoSTEM-EDX was completed to extract the composition at a nanometre scale. The general trend of the nanoSTEM-EDX spectra is similar for all samples, displaying a large composition inhomogeneity. More nanoSTEM-EDX data are presented in ESI, Fig. S6–S9†, and while single nPs nanoSTEM-EDX data vary strongly, nPs still appear systematically to be Pt rich. In contrast, the film like material is consistently characterized as Fe rich regardless of the initial iron to platinum salt ratio used for the syntheses.[59]

Table 1 XRD data of FePt nPs synthesized at 30 °C in isooctane, [Brij52] = 0.3 mol L^{-1}, [Brij52]/[butanol] = 5, w = 4, $[K_2PtCl_4]$ = 2.5 mmol L^{-1}, $[N_2H_4 \cdot H_2O]/[Fe^{3+} + Pt^{2+}]$ = 40. a is the lattice constant deduced from the (111), (200) and (220) peak positions, x is the iron content in Fe_xPt_{1-x}, the diameter D_{XRD} is the crystalline grain size calculated based on FWHM of 3 different XRD peaks[59]

Fe/Pt salt ratio	a/Å	x (%)	D_{XRD}/nm
0.2	3.906 ± 0.006	17.4 ± 4.3	6.2 ± 1.2
0.6	3.908 ± 0.006	15.6 ± 4.4	6.4 ± 0.8
1.0	3.911 ± 0.005	13.2 ± 3.6	7.3 ± 0.5
1.4	3.911 ± 0.002	13.0 ± 1.2	8.5 ± 1.0
1.8	3.910 ± 0.004	14.0 ± 3.1	9.2 ± 1.4

Discussion

Colloidal syntheses might not be as straightforward and simple as one could believe when scanning through the literature and

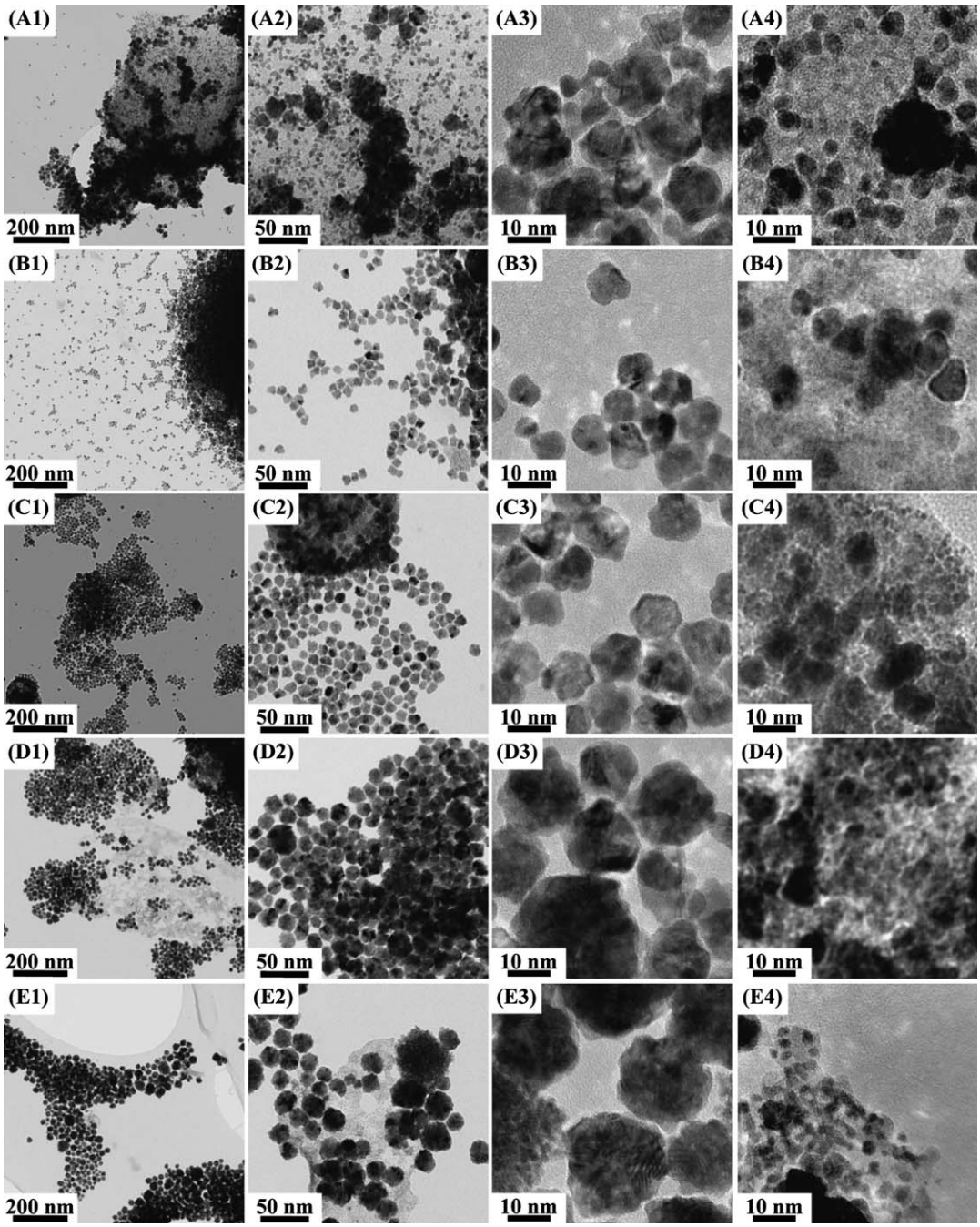

Fig. 3 TEM images of as-synthesized FePt nPs synthesized at 30 °C in isooctane, [Brij52] = 0.3 mol L^{-1}, [Brij52]/[butanol] = 5, $w = 4$, [K_2PtCl_4] = 2.5 mmol L^{-1} and [$N_2H_4 \cdot H_2O$]/[Fe^{3+} + Pt^{2+}] = 40. [$FeCl_3$] to [K_2PtCl_4] molar ratio: 0.2 (A), 0.6 (B), 1.0 (C), 1.4 (D) and 1.8 (E).

only very recently have some researchers started to report on, sometimes substantial, result deviations from data published by others or even by the very same research group. Noticeable examples include the effect of TOPO associated impurities on CdSe synthesis *via* a widely used thermal decomposition pathway,[61,62] the effect of CTAB impurity associated with the synthesis of Ag nanorods,[63] the effect of NaCl traces in ethylene glycol used to obtain Ag nanocubes through a polyol protocol,[64] or the influence of oleate complex on iron oxide nanoparticles.[65] The list is not exhaustive and this should not be a surprise as the systems to be played with can arguably be more complex than they appear. Slight changes of protocol, experimental setup, provider if not chemical batch lead to potentially very different products which are also characterised differently from one publication to another, hence sometimes preventing direct comparison. These later reports might, however, contain significantly more scientific insights paving the way to reproducible syntheses. In the context of FePt, the material presently of interest, homogeneous chemical composition is a key requirement for both basic and technological investigations to be completed with alloyed nPs and for low temperature syntheses of FePt nPs to be used, this major challenge needs to be addressed.

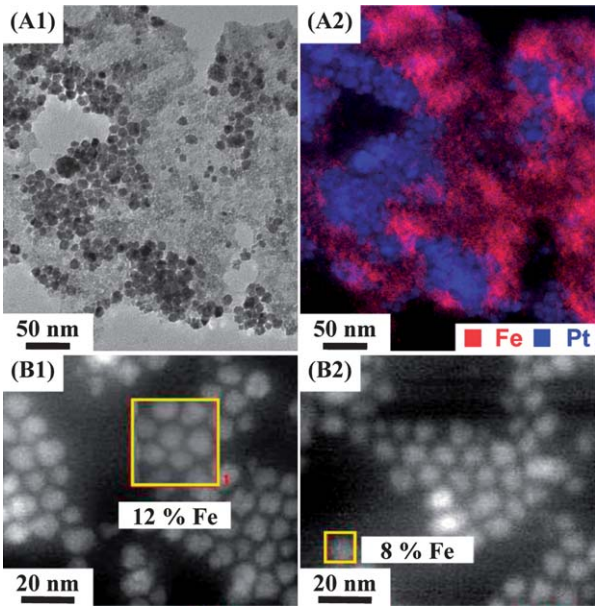

Fig. 4 Bright field TEM picture (A1) and corresponding EFTEM image showing Pt in blue and Fe in red (A2). Dark field nanoSTEM-EDX data (B1 and B2) of FePt nPs synthesized at 30 °C in isooctane, [Brij52] = 0.3 mol L^{-1}, [Brij52]/[butanol] = 5, w = 4, $[N_2H_4{\cdot}H_2O]/[Fe^{3+} + Pt^{2+}]$ = 40, molar ratio of Fe : Pt precursors = 1.

To summarize the data presented so far, FePt nPs syntheses were carried out with $FeCl_3/K_2PtCl_4$/hydrazine monohydrate in water/isooctane/Brij52/butanol amphiphilic system. The hydration of 4 molecules of water per molecule of surfactant was chosen to have maximum conductivity, *i.e.* higher exchange rate, throughout the system. The knobbly appearance of the nPs suggests their formation follows a two-stage growth mechanism in which nanocrystals first nucleate in a supersaturated solution and next grow by both aggregating and fusing to form larger particles. The size of nPs increases with the Fe to Pt precursor ratio in the synthesis media. However, the combination of characterization techniques including ICP-OES (Fig. 2A), XRD (Fig. 2B and Table 1), TEM (Fig. 3), EFTEM (Fig. 4A) and nanoSTEM-EDX (Fig. 4B) reveals that the nPs composition is strongly inhomogeneous, Pt rich, and that it could not be tuned by changing the initial Fe to Pt precursor ratio.

Assuming that $FeCl_3$ and K_2PtCl_4 could be reduced at very different rates or that $FeCl_3$ could hydrolyze to insoluble and unreactive oxohydroxo species, a number of strategies were explored with the aim of identifying limiting factors:

(1) The potential formation of an iron 'richer' shell is investigated by considering the effect of the reaction time on the nPs.

(2) The effect of Fe and Pt salts on the nPs composition is investigated as more hydrolytically stable iron precursors should give higher incorporation of iron into the nPs.

(3) By competing with the hydrolysis of the iron precursor, a stronger reducing agent might allow greater Fe incorporation into the nPs. The use of sodium borohydride is then discussed as hydrazine monohydrate is known as having moderate efficiency in reducing $FeCl_3$.[66,67]

The reaction time was varied from 0.25 h to 16 h to assess the effect of time on the Fe incorporation into the nPs. There was very little change in the composition of the nPs and the only slight effect was for the Pt rich nPs to become slightly larger at longer times, growing by aggregation or Oswald ripening type of processes. This is consistent with the $FeCl_3$ having hydrolyzed and the K_2PtCl_4 having been reduced during the very early stages of the reaction (Section III.2, ESI†).[59]

Chlorine and oxygen found in the iron rich materials (ESI, Fig. S6–S9†) suggest incomplete $FeCl_3$ reduction or the formation of akaganeite (β-FeOOH),[59] which results from the hydrolysis of Fe^{3+} in aqueous solution and is favored by the presence of chloride ion.[68,69] It is known that $FeCl_3$ hydrolyses to $[Fe(OH_2)_6]^{3+}$ in the presence of water, while the high charge to radius ratio in Fe^{3+} induces deprotonation leading, *via* olation and oxolation, to oxobridged iron species which precipitate as 2–4 nm spheres containing $\sim 10^2$ Fe^{III} ions, most likely in octahedral $Fe(O,OH,H_2O)_6$ coordination.[68] In addition, the reduction strength of hydrazine is know to be weakened by the decreasing pH,[66] which can be afforded by the deprotonation of the $[Fe(OH_2)_6]^{3+}$. Such a pH decrease down to 1.2 was observed when the $FeCl_3$ concentration was increased (ESI, Table S1†).[59] Thus, the hydrolysis of $FeCl_3$ in the presence of hydrazine can lead to insoluble ion salts, which prevent the Fe ions from reacting with the platinum salts or the initially formed Pt clusters; at a later stage, this would also prevent the formation of a Fe rich shell surrounding Pt rich nPs. The validity of this hypothesis is explored in the following section. In contrast, $[PtCl_2(H_2O)_2]$ complexes can be formed through hydrolysis of $[PtCl_4]^{2-}$ but precipitation of platinum does not occur. The hydrolysis reaction of $[PtCl_4]^{2-}$ is shown in eqn (1) and (2).[70]

$$[PtCl_4]^{2-} + H_2O \leftrightarrow [PtCl_3(H_2O)]^- + Cl^- \quad (1)$$

$$[PtCl_3(H_2O)]^- + H_2O \leftrightarrow [PtCl_2(H_2O)_2] + Cl^- \quad (2)$$

A $[PtCl_2(H_2O)_2]$ Pt^{II} complex can be reduced to form a Pt^{I} complex by the introduction of one electron. The Pt^{I} complex can react with the unreduced Pt^{II} complex to form a Pt^{I}-Pt^{II} dimer.[70–72] A Pt^{I}–Pt^{I} dimer can be further formed through the addition of another electron to the Pt^{I}–Pt^{II} dimer. Both dimers can react with a third $[PtCl_2(H_2O)_2]$ complex to form a trimer. These partially reduced dimers and trimers probably represent early intermediates toward the formation of larger clusters or nuclei from which the nPs grow. Dimers and trimers have higher electron affinities than the original Pt precursor due to orbital delocalization, reduction is then expected to occur preferentially *via* electron transfer from the reductant to these dimeric and trimeric units.[71,72] It would be tempting to associate such material with the small nPs of light contrast, observed in larger amount in HR-TEM image of molar ratio 1.8 sample (Fig. 3—4th column). This would provide further evidence to indicate that it is the hydrolysis of $FeCl_3$ which leads to the film-like material. However, their small diameter of 2 nm can only provide broad XRD peaks, which, in the present work, cannot be discernible from the background.

While synthesizing alloyed nanoparticles, the effects of mixing the salt precursors also need to be considered. Indeed, K_2PtCl_6 can form when mixing $FeCl_3$ and K_2PtCl_4 salts in aqueous solution, leading to insoluble yellow crystals (ESI, Fig. S10A†).[59] Whereas K_2PtCl_6 precipitates are dissolved when hydrazine is added to the aqueous solution, their formation could contribute to the observed inhomogeneous nucleation of Pt and Fe

materials. This was investigated by using Na_2PtCl_6 as a Pt source. In addition and as indicated above, a major problem with the use of aqueous systems is that $FeCl_3$ hydrolyses rapidly to insoluble oxyhydroxide species, but it is well known that Fe^{II} is less hydrolytically unstable because of the lower charge to radius ratio. In addition Fe^{II} salts will not react with K_2PtCl_4 to give K_2PtCl_6. Therefore, the effect of Fe^{II} precursors, Fe(acetate)$_2$ and $FeCl_2$ as well as Fe^{III} salts free of chlorine atoms like $Fe(NO_3)_3$ was investigated. The XRD characterization of the products then formed is summarized in Table 2 and the original XRD patterns can be found in ESI, Fig. S10C†.[59]

Whereas the platinum precursor does not have much impact, the crystalline grain sizes of Fe^{2+} samples are smaller than Fe^{3+} samples, reaching 2.6 nm in diameter with $FeCl_2$ compared to 7.4 nm with $FeCl_3$ for instance, a variation much larger than the experimental uncertainty. Similarly, regardless of the Pt precursors, all Fe^{3+} precursor based samples have a similar lattice constant, corresponding to ~15% Fe composition. Strikingly though, Fe^{2+} precursors are associated with an increase of the Fe insertion into the nPs by more than 60% and 150% for Fe(acetate)$_2$ and $FeCl_2$, respectively. The general trend of increased iron insertion into the nPs can be explained by greater hydrolytic stability of Fe^{2+} precursors, but may also be influenced by the lower reduction potential of $Fe^{II/0}$ compared with $Fe^{III/0}$ (ESI, Table S2†).[59] The difference between Fe(acetate)$_2$ and $FeCl_2$ could result from the different dissociation constants associated with the acetate and the chlorine salts. For all precursors, TEM reveals similar typical features as previously highlighted including the presence of both nPs which show a multidomain structure and film like materials (Fig. 5). Slight variations of the nPs size can be observed while the apparent variation remains smaller than with the crystalline grain size presented in Table 2. The multidomain feature is stronger for the synthesis completed with $FeCl_2$ and K_2PtCl_4 (Fig. 5D1), which is also associated with the smallest crystalline grain size of about 2.5 nm in diameter. Larger length scale TEM images and nanoSTEM-EDX results are presented in the 2nd column of Fig. 5, with the main features being the large inhomogeneous distribution of Fe and Pt materials together with the coexistence of Pt rich nPs with Fe rich film-like material. This is observed regardless of the precursor set.

To sum up the results associated with the strategy #2, while the formation of K_2PtCl_6 can be avoided by changing Pt and Fe precursors, the oxidation state of the Fe ions is identified as the most important parameter for increasing the iron content in the alloyed FePt nPs. Fe^{2+} ions are more stable to hydrolysis and hence remain available for reduction to Fe^0 and incorporation into the nPs increasing the iron content up to ~34% (Table 2).

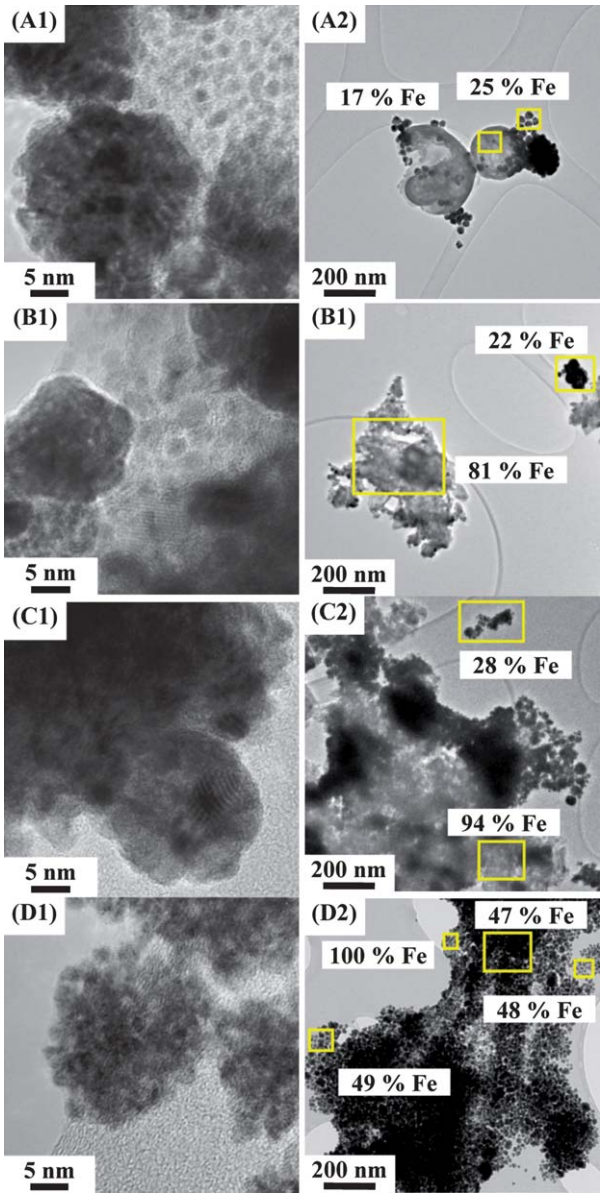

Fig. 5 TEM images of FePt nPs synthesized at 30 °C in isooctane, [Brij52] = 0.3 mol L^{-1}, [Brij52]/[butanol] = 5, w = 4, [$Fe^{3+/2+}$] = [Pt^{2+}] = 2.5 mmol L^{-1} and $N_2H_4{\cdot}H_2O$ as reducing agent at a ratio of [$N_2H_4{\cdot}H_2O$]/[$Fe^{3+/2+}$ + Pt^{2+}] = 40 and different precursors $FeCl_3$ and Na_2PtCl_6 (A), $Fe(NO_3)_3$ and K_2PtCl_4 (B), Fe(acetate)$_2$ and K_2PtCl_4 (C), $FeCl_2$ and K_2PtCl_4 (D).

Table 2 XRD data of FePt nPs synthesized with different Fe and Pt precursors at 30 °C in isooctane, [Brij52] = 0.3 mol L^{-1}, [Brij52]/[butanol] = 5, w = 4, [$Fe^{2+/3+}$] = [Pt^{2+}] = 2.5 mmol L^{-1} and [$N_2H_4{\cdot}H_2O$]/[$Fe^{2+/3+}$ + Pt^{2+}] = 40. a is the lattice constant, x is the iron content in Fe_xPt_{1-x}, the diameter D_{XRD} is the crystalline grain size.[59]

Precursors	a/Å	x (%)	D_{XRD}/nm
$FeCl_3/K_2PtCl_4$	3.911 ± 0.005	13.2 ± 3.6	7.3 ± 0.5
$FeCl_3/Na_2PtCl_6$	3.910 ± 0.006	15.0 ± 1.3	8.8 ± 1.4
$Fe(NO_3)_3/K_2PtCl_4$	3.911 ± 0.005	13.3 ± 3.6	7.4 ± 1.8
Fe(acetate)$_2$/K_2PtCl_4	3.899 ± 0.003	21.5 ± 2.2	5.8 ± 1.1
$FeCl_2/K_2PtCl_4$	3.882 ± 0.005	33.9 ± 3.4	2.6 ± 0.5

$NaBH_4$ is a much stronger reducing agent than hydrazine monohydrate (ESI, Table S1†),[59,73] which is commonly used for the synthesis of nanomaterials. Marcus theory and experimental results for a large range of nanoparticles suggest that it is also a faster reducing agent implying that the reduction to Fe^0 may then become competitive with the hydrolysis reaction.

The XRD characterization presented in Table 3 and in ESI, Fig. S10C and D† shows that the crystalline grain size remains constant within the experimental uncertainty with both the reducing agent ratio and the reactivity of the iron precursor.[59]

This prevents further discussion regarding the nucleation rate associated with a fast reduction. Compared to hydrazine, the XRD peak positions are shifted towards higher 2θ values (ESI, Fig. S10C and D†),[59] corresponding to a decrease of the lattice spacing and a concomitant higher Fe content, up to 35%. This value is similar to the 34% value obtained with $FeCl_2/K_2PtCl_4/N_2H_4 \cdot H_2O$, supporting a kinetic related strategy is appropriate to co-reduce Fe and Pt precursors simultaneously, but also implying that a limit to Fe insertion may have been reached.

Pt segregation at the surface of the FePt alloy particles would cause significant composition gradient from the core and hence could change the apparent cell parameters even if the overall composition was fixed; this effect is particularly pronounced for small particles with a larger surface area. However, in the case of this study, Pt atoms still appear to react faster than Fe precursors, the XRD peak positions are consistently shifted towards higher 2θ values and magnetic measurements show that the 35% Fe nPs have a stronger magnetic moment than the 15% Fe nPs (ESI, Fig. S12†),[59] which then preclude the hypothesis of Pt segregation at the surface of nPs. It is noticeable that the formation of Pt rich nPs explains why the magnetization does not reach saturation at temperatures below T_b, along with the weak coercivity of the present nPs,[59] when compared with the FePt nPs literature.[23,31,34] Fig. 6A1 and B1 are typical TEM images and fully consistent with the data previously presented showing both knobbly nPs and thin-film like material. NanoTEM-EDX demonstrates once again the inhomogeneous distribution of Fe and Pt regardless of the iron precursor being used (Fig. 6A2 and B2).

Consequently, it can be deduced not only that it is possible to increase the iron content in the nPs but also that aqueous media induced a limit to the Fe content which could be inserted into the alloyed iron–platinum magnetic nPs. This demonstration relies on strategies aiming at increasing the reduction rate of the iron ions and decreasing the hydrolysis of the Fe precursor. From that perspective rather than a limitation of amphiphilic systems, our results highlight what appears to be a limitation of the co-reduction method to form alloyed nPs when water is present. These results then imply that future efforts should focus on overcoming the formation of hydrolytically unstable iron complexes to develop low temperature co-reduction syntheses of FePt nPs with homogenous chemical composition. This could best be achieved by eliminating water entirely from the system or designing appropriate precursors. Tuning the size of the product obtained in non-aqueous media and more specifically increasing the size of the nPs might then later be achieved by decreasing the reduction rate difference between the two precursors.

Table 3 XRD data of FePt nPs synthesized at 30 °C in isooctane, [Brij52] = 0.3 mol L^{-1}, [Brij52]/[butanol] = 5, w = 4, $[Fe^{3+/2+}]$ = $[K_2PtCl_4]$ = 2.5 mmol L^{-1} and $[NaBH_4]/[Fe^{3+/2+} + Pt^{2+}]$ = 2.5, 5 and 10. a is the lattice constant, x is the iron content in Fe_xPt_{1-x}, the diameter D_{XRD} is the crystalline grain size.[59] (a) $FeCl_3/K_2PtCl_4/NaBH_4$, (b) $FeCl_2/K_2PtCl_4/NaBH_4$.

	Ratio	a/Å	x (%)	D_{XRD}/nm
(a)	2.5	3.887 ± 0.005	30.2 ± 3.3	4.0 ± 0.7
	5.0	3.881 ± 0.002	34.6 ± 1.3	3.5 ± 0.5
	10.0	3.880 ± 0.005	35.6 ± 3.4	3.2 ± 0.7
(b)	5.0	3.882 ± 0.003	34.4 ± 2.1	3.5 ± 0.7

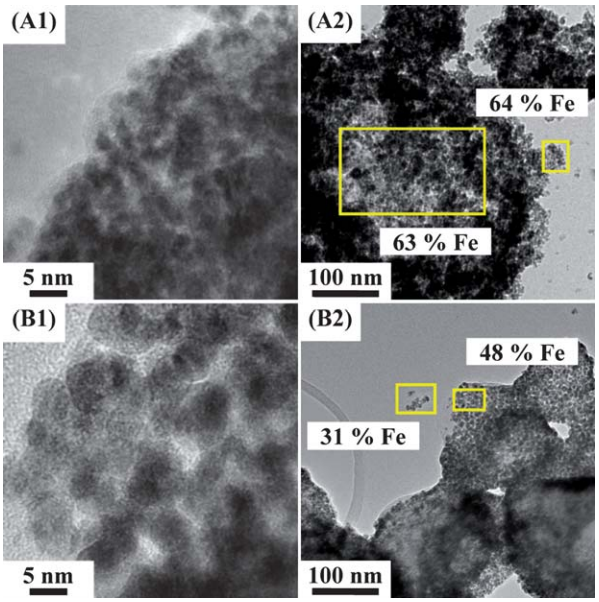

Fig. 6 TEM images of FePt nPs synthesized at 30 °C in isooctane, [Brij52] = 0.3 mol L^{-1}, [Brij52]/[butanol] = 5, w = 4, $[Fe^{3+/2+}] = [Pt^{2+}]$ = 2.5 mmol L^{-1} and $NaBH_4$ as reducing agent with $[NaBH_4]/[Fe^{3+/2+} + Pt^{2+}]$ = 5: (A) $FeCl_3$ and K_2PtCl_4 and (B) $FeCl_2$ and K_2PtCl_4.

Conclusion

The goal of this study was to understand the effect of ionic precursors and reducing agents on the composition of alloyed nanomaterials synthesized at low temperature to identify suitable strategies to overcome the problem of the product compositional inhomogeneity. Fe_xPt_{1-x} alloy nPs were synthesized in a non-ionic amphiphilic system made of water, isooctane, Brij52 and butanol, characterized by impedance spectroscopy. By combining characterization techniques including ICP-OES, XRD, and nanoTEM-EDX, this investigation highlights a two-stage growth mechanism of the nPs. Primary nanocrystals first nucleate in a supersaturated solution and then keep on growing and coalescing into larger knobbly particles. Multidomain Pt rich nPs are already formed after 15 min of synthesis. While excess of Fe is found in the film-like material, extending the reaction time up to 16 h leads to larger nPs but does not alter the nPs Fe to Pt ratio because the competitive hydrolysis of the iron precursors is completed within 15 min. This was confirmed by using the faster reducing agent, $NaBH_4$, and the less hydrolytically unstable Fe^{II} precursors which both increased the iron content of the nanoparticles from ~15% to ~34%. We then demonstrate that in order to obtain higher stoichiometry in FePt nPs by co-reduction at low temperature, the formation of hydrolytically unstable iron complexes needs to be overcome while the difference in the reduction rate needs to be reduced or offset by a strong reducing agent. This strategy may allow low temperature synthesis to become an advantageous route to the production of FePt nPs targeting applications including data storage technology and biomedicine. The limiting parameters

and strategy we highlight here will be applicable to the fabrication of other alloyed nanomaterials.

Acknowledgements

The authors gratefully acknowledge the *Scottish Universities Physics Alliance* for funding of Dr Pascal André's and Dr Donald MacLaren's *SUPA Advanced Research Fellowships*, the *James and Enid Nicol Trust* for funding Shu Chen's studentship. The authors would like to thank Dr S. Song for help with impedance measurements, Dr Lorna Eades (*EaStCHEM—University of Edinburgh*) for the ICP-OES measurements, Prof P. Bruce (*University of St Andrews*) to access XRD instrument. PA and SC would like to thank C. Booth, J. Lindsay, M. Ross and D. Steven from the Electronic and Mechanical workshops (*School of Physics and Astronomy* at *St Andrews*) for their assistance while designing the impedance cell.

Notes and references

1 Y. Xia, Y. J. Xiong, B. Lim and S. E. Skrabalak, *Angew. Chem., Int. Ed.*, 2009, **48**, 60–103.
2 D. V. Talapin, J. S. Lee, M. V. Kovalenko and E. V. Shevchenko, *Chem. Rev.*, 2010, **110**, 389–458.
3 M. C. Daniel and D. Astruc, *Chem. Rev.*, 2004, **104**, 293–346.
4 A. H. Lu, E. L. Salabas and F. Schuth, *Angew. Chem., Int. Ed.*, 2007, **46**, 1222–1244.
5 L. S. Nair and C. T. Laurencin, *J. Biomed. Nanotechnol.*, 2007, **3**, 301–316.
6 U. Jeong, X. W. Teng, Y. Wang, H. Yang and Y. N. Xia, *Adv. Mater.*, 2007, **19**, 33–60.
7 I. L. Medintz, H. T. Uyeda, E. R. Goldman and H. Mattoussi, *Nat. Mater.*, 2005, **4**, 435–446.
8 S. H. Sun, *Adv. Mater.*, 2006, **18**, 393–403.
9 J. Kim, Y. Lee and S. H. Sun, *J. Am. Chem. Soc.*, 2010, **132**, 4996–4997.
10 J. P. Wang, *Proc. IEEE*, 2008, **96**, 1847–1863.
11 V. I. Shubayev, T. R. Pisanic and S. H. Jin, *Adv. Drug Delivery Rev.*, 2009, **61**, 467–477.
12 H. B. Na, I. C. Song and T. Hyeon, *Adv. Mater.*, 2009, **21**, 2133–2148.
13 O. Veiseh, J. W. Gunn and M. Q. Zhang, *Adv. Drug Delivery Rev.*, 2010, **62**, 284–304.
14 R. Bhattacharya and P. Mukherjee, *Adv. Drug Delivery Rev.*, 2008, **60**, 1289–1306.
15 J. H. Gao and B. Xu, *Nano Today*, 2009, **4**, 37–51.
16 J. H. Gao, H. W. Gu and B. Xu, *Acc. Chem. Res.*, 2009, **42**, 1097–1107.
17 J. H. Gao, G. L. Liang, J. S. Cheung, Y. Pan, Y. Kuang, F. Zhao, B. Zhang, X. X. Zhang, E. X. Wu and B. Xu, *J. Am. Chem. Soc.*, 2008, **130**, 11828–11833.
18 S. Chen, L. J. Wang, S. L. Duce, S. Brown, S. Lee, A. Melzer, S. A. Cuschieri and P. Andre, *J. Am. Chem. Soc.*, 2010, **132**, 15022–15029.
19 Q. A. Pankhurst, J. Connolly, S. K. Jones and J. Dobson, *J. Phys. D: Appl. Phys.*, 2003, **36**, R167–R181.
20 O. Gutfleisch, J. Lyubina, K. H. Muller and L. Schultz, *Adv. Eng. Mater.*, 2005, **7**, 208–212.
21 S. S. Kang, Z. Y. Jia, S. F. Shi, D. E. Nikles and J. W. Harrell, *Appl. Phys. Lett.*, 2005, **86**, 062503.
22 Y. H. Huang, Y. Zhang, G. C. Hadjipanayis and D. Weller, *J. Appl. Phys.*, 2003, **93**, 7172–7174.
23 S. Sun, C. B. Murray, D. Weller, L. Folks and A. Moser, *Science*, 2000, **287**, 1989–1992.
24 J. A. Christodoulides, M. J. Bonder, Y. Huang, Y. Zhang, S. Stoyanov, G. C. Hadjipanayis, A. Simopoulos and D. Weller, *Phys. Rev. B: Condens. MatterMater. Phys.*, 2003, **68**, 054428.
25 A. C. C. Yu, M. Mizuno, Y. Sasaki and H. Kondo, *Appl. Phys. Lett.*, 2004, **85**, 6242–6244.
26 M. Takahashi, T. Ogawa, D. Hasegawa and B. Jeyadevan, *J. Appl. Phys.*, 2005, **97**, 10J307.
27 J. M. Kim, C. B. Rong, J. P. Liu and S. H. Sun, *Adv. Mater.*, 2009, **21**, 906–909.
28 N. Caiulo, C. H. Yu, K. M. K. Yu, C. C. H. Lo, W. Oduro, B. Thiebaut, P. Bishop and S. C. Tsang, *Adv. Funct. Mater.*, 2007, **17**, 1392–1396.
29 C. B. Rong, D. R. Li, V. Nandwana, N. Poudyal, Y. Ding, Z. L. Wang, H. Zeng and J. P. Liu, *Adv. Mater.*, 2006, **18**, 2984–2988.
30 Z. R. Dai, S. H. Sun and Z. L. Wang, *Nano Lett.*, 2001, **1**, 443–447.
31 H. L. Nguyen, L. E. M. Howard, G. W. Stinton, S. R. Giblin, B. K. Tanner, I. Terry, A. K. Hughes, I. M. Ross, A. Serres and J. S. O. Evans, *Chem. Mater.*, 2006, **18**, 6414–6424.
32 S. Saita and S. Maenosono, *Chem. Mater.*, 2005, **17**, 6624–6634.
33 M. Chen, J. P. Liu and S. Sun, *J. Am. Chem. Soc.*, 2004, **126**, 8394–8395.
34 V. Nandwana, K. E. Elkins, N. Poudyal, G. S. Chaubey, K. Yano and J. P. Liu, *J. Phys. Chem. C*, 2007, **111**, 4185–4189.
35 E. V. Shevchenko, D. V. Talapin, H. Schnablegger, A. Kornowski, O. Festin, P. Svedlindh, M. Haase and H. Weller, *J. Am. Chem. Soc.*, 2003, **125**, 9090–9101.
36 M. Delalande, P. R. Marcoux, P. Reiss and Y. Samson, *J. Mater. Chem.*, 2007, **17**, 1579–1588.
37 J. Eastoe and A. R. Cox, *Colloids Surf., A*, 1995, **101**, 63–76.
38 A. Filankembo and M. P. Pileni, *Appl. Surf. Sci.*, 2000, **164**, 260–267.
39 N. Pinna, K. Weiss, H. Sack-Kongehl, W. Vogel, J. Urban and M. P. Pileni, *Langmuir*, 2001, **17**, 7982–7987.
40 P. André, F. Charra, P. A. Chollet and M. P. Pileni, *Adv. Mater.*, 2002, **14**, 601–603.
41 A. Filankembo, S. Giorgio, I. Lisiecki and M. P. Pileni, *J. Phys. Chem. B*, 2003, **107**, 7492–7500.
42 M. Maillard, S. Giorgio and M. P. Pileni, *J. Phys. Chem. B*, 2003, **107**, 2466–2470.
43 R. D. Tilley, J. H. Warner, K. Yamamoto, I. Matsui and H. Fujimori, *Chem. Commun.*, 2005, 1833–1835.
44 J. Park, J. Joo, S. G. Kwon, Y. Jang and T. Hyeon, *Angew. Chem., Int. Ed.*, 2007, **46**, 4630–4660.
45 Z. Y. Li, J. P. Wilcoxon, F. Yin, Y. Chen, R. E. Palmer and R. L. Johnston, *FaradayDiscuss.*, 2008, **138**, 363–373.
46 B. Abecassis, F. Testard and T. Zemb, *Soft Matter*, 2009, **5**, 974–978.
47 A. K. Ganguli, A. Ganguly and S. Vaidya, *Chem. Soc. Rev.*, 2010, **39**, 474–485.
48 S. H. Xuan, F. Wang, Y. X. J. Wang, J. C. Yu and K. C. F. Leung, *J. Mater. Chem.*, 2010, **20**, 5086–5094.
49 J. P. Cason, M. E. Miller, J. B. Thompson and C. B. Roberts, *J. Phys. Chem. B*, 2001, **105**, 2297–2302.
50 B. L. Cushing, V. L. Kolesnichenko and C. J. O'Connor, *Chem. Rev.*, 2004, **104**, 3893–3946.
51 M. Nakanishi, G. I. Furusawa, K. Waki, Y. Hattori, T. Kamino, K. Sasaki, K. Kuroda and H. Saka, *Mater. Trans.*, 2007, **48**, 2572–2579.
52 L. T. Bai, H. Y. Wan and S. C. Street, *Colloids Surf., A*, 2009, **349**, 23–28.
53 E. E. Carpenter, J. A. Sims, J. A. Wienmann, W. L. Zhou and C. J. O'Connor, *J. Appl. Phys.*, 2000, **87**, 5615–5617.
54 K. M. Hyie and I. D. Yaacob, *J. Mater. Process. Technol.*, 2007, **191**, 48–50.
55 Q. Y. Yan, A. Purkayastha, T. Kim, R. Kroger, A. Bose and G. Ramanath, *Adv. Mater.*, 2006, **18**, 2569–2573.
56 Y. Gao, X. W. Zhang, Z. G. Yin, S. Qu, J. B. You and N. F. Chen, *Nanoscale Res. Lett.*, 2010, **5**, 1–6.
57 B. D. Reiss, C. B. Mao, D. J. Solis, K. S. Ryan, T. Thomson and A. M. Belcher, *Nano Lett.*, 2004, **4**, 1127–1132.
58 S. Qu, X. W. Zhang, Y. Gao, J. B. You, Y. M. Fan, Z. G. Yin and N. F. Chen, *Nanotechnology*, 2008, **19**, 135704.
59 See ESI† for details.
60 J. W. A. Bonakdarpour, D. A. Stevens, S. Sheng, T. L. Monchesky, R. Löbel, R. T. Atanasoski, A. K. Schmoeckel, G. D. Vernstrom, M. K. Debe and J. R. Dahna, *J. Electrochem. Soc.*, 2005, **152**, A61–A72.
61 F. Wang, R. Tang, J. L. F. Kao, S. D. Dingman and W. E. Buhro, *J. Am. Chem. Soc.*, 2009, **131**, 4983–4994.
62 F. D. Wang, R. Tang and W. E. Buhro, *Nano Lett.*, 2008, **8**, 3521–3524.
63 N. J. Durr, T. Larson, D. K. Smith, B. A. Korgel, K. Sokolov and A. Ben-Yakar, *Nano Lett.*, 2007, **7**, 941–945.

64 B. Wiley, T. Herricks, Y. G. Sun and Y. N. Xia, *Nano Lett.*, 2004, **4**, 1733–1739.
65 L. M. Bronstein, X. L. Huang, J. Retrum, A. Schmucker, M. Pink, B. D. Stein and B. Dragnea, *Chem. Mater.*, 2007, **19**, 3624–3632.
66 C. L. Yang, J. M. Xing, Y. P. Guan, J. G. Liu and H. Z. Liu, *J. Alloys Compd.*, 2004, **385**, 283–287.
67 H. Iida, T. Nakanishi, H. Takada and T. Osaka, *Electrochim. Acta*, 2006, **52**, 292–296.
68 C. M. Flynn, *Chem. Rev.*, 1984, **84**, 31–41.
69 P. Refait and J. M. R. Genin, *Corros. Sci.*, 1997, **39**, 539–553.
70 C. I. Sanders and D. S. Martin, *J. Am. Chem. Soc.*, 1961, **83**, 807–810.
71 L. C. Ciacchi, W. Pompe and A. De Vita, *J. Am. Chem. Soc.*, 2001, **123**, 7371–7380.
72 L. C. Ciacchi, W. Pompe and A. De Vita, *J. Phys. Chem. B*, 2003, **107**, 1755–1764.
73 Anhydrous hydrazine was not used in the present study as the chemical is not commercially available outside the USA and obtaining it from the distillation of hydrazine monohydrate presents risks associated with the explosive properties of the compound.

